A general optimization strategy for composite sandwich structures

François-Xavier Irisarri, Cédric Julien, Dimitri Bettebghor, Florian Lavelle, Yannick Guerin, Kevin Mathis

Structural and Multidisciplinary Optimization manuscript No.
(will be inserted by the editor)

A general optimization strategy for composite sandwich structures

François-Xavier Irisarri · Cédric Julien · Dimitri Bettebghor · Florian Lavelle · Yannick Guerin · Kevin Mathis

Received: date / Accepted: date

Abstract An original strategy for the design of large-scale composite sandwich structures is developed. Such structures are typical of launcher and spacecraft structures, but the methodology remains applicable to any thin-walled sandwich structure (such as aircraft fuselage panels or watercraft hulls). The method hinges on multi-step strategies devised for variable-stiffness laminates. Indeed, laminate optimization problems corresponds to large combinatorial design spaces and their efficient approximate solutions often combine continuous relaxation and metaheuristics. Typically, the first step consists of a gradient-based optimization that handles the large number of variables with a continuous representation of the composite mechanical behavior. In our work, this continuous representation is adapted to the specific features of laminated sandwich composites. In particular, we modeled the dependency of the material transverse shear stiffness on the design variables (composite skins and core) by employing a machine learning based approximation. The face sheet laminates are then determined in a second step using an evolutionary algorithm with stacking sequence tables to represent thickness variations. Finally, we introduce a third optimization step to overcome the design feasibility issues related to the use of a stiffness matching method for the determination of the layups of the face sheet laminates. The method is applied to the minimization of the overall weight of a load-carrying structure similar to the Ariane 5 dual-launch system, under several launcher-specific mechanical constraints.

F.-X. Irisarri
DMAS, ONERA, Université Paris Saclay, F-92322 Châtillon, France
E-mail: francois-xavier.irisarri@onera.fr

C. Julien
DMAS, ONERA, Université Paris Saclay, F-92322 Châtillon, France
E-mail: cedric.julien@onera.fr

D. Bettebghor
DMAS, ONERA, Université Paris Saclay, F-92322 Châtillon, France
E-mail: dimitri.bettebghor@onera.fr

F. Lavelle
CNES, Direction des Lanceurs, F-75012 Paris, France
E-mail: florian.lavelle@cnes.fr

Y. Guerin
CNES, Direction des Lanceurs, F-75012 Paris, France
E-mail: yannick.guerin@cnes.fr

K. Mathis
CNES, Direction des Lanceurs, F-75012 Paris, France
E-mail: kevin.mathis@cnes.fr

Keywords Composite laminate · Lamination parameters · Transverse shear stiffness · Multi-step optimization

Nomenclature

m	=	total mass of the structure
t_c	=	sandwich core thickness
t_s	=	sandwich skin thickness
t_p	=	elementary layer thickness
$\boldsymbol{\theta}$	=	ply orientations of a skin laminate
n	=	number of layers in a skin laminate
$\mathrm{V}^{\mathrm{A,B,D}}_{i=1,\dots,4}$	=	in-plane, coupling and bending lamination parameters
$\mathbf{A}$	=	membrane stiffness matrix
$\mathbf{B}$	=	membrane/bending coupling stiffness matrix
$\mathbf{D}$	=	bending stiffness matrix
$\mathbf{F}$	=	transverse shear stiffness matrix
$\mathbf{N}$	=	membrane forces
$\mathbf{M}$	=	bending moments
$\mathbf{T}$	=	transverse shear forces
$\boldsymbol{\varepsilon}^{\mathbf{0}}$	=	in-plane strains of the laminate midplane
$\boldsymbol{\kappa}$	=	curvatures of the laminate midplane
$\boldsymbol{\gamma}$	=	transverse strains of the laminate midplane
$\mathbf{Q}$	=	reduced stiffness matrix of the ply
$\boldsymbol{\Gamma}_{\mathbf{i=0,\dots,4}}$	=	in-plane material parameters of the ply
$\boldsymbol{\Lambda}_{\mathbf{i=0,\dots,2}}$	=	transverse material parameters of the ply
$\mathbf{g}$	=	mechanical design constraints
$\mathbf{q}$	=	laminate design guidelines
$d(\mathrm{A}_1, \mathrm{A}_2)$	=	KL-divergence between matrices $\mathbf{A}_1$ and $\mathbf{A}_2$
$\mathrm{K}_{\mathrm{F}z}$, $\mathrm{K}_{\mathrm{F}y}$, $\mathrm{K}_{\mathrm{M}x}$	=	SYLDA global stiffness components
λ_i	=	i-th buckling factor

1 Introduction

Carbon fiber reinforced plastics (CFRP) are widely used in launcher structures. Many critical parts are made of sandwich materials with CFRP skins and honeycomb or foam core material. In particular, most launcher structures are typically quite large and are cylindrically or conically shaped, so that using skins with a variable thickness is often the most efficient way to minimize their overall mass. Designing such structures, however, is a challenging task.

While the literature about the optimization of CFRP monolithic structures is extensive [17,16,4], articles dealing with the optimal design of laminated sandwich composites are less abundant. Classical design of sandwich structures focuses on the optimization of the thickness of the core and metallic face sheets with fixed materials [5,20]. The method was later adapted to composite skins using one thickness design variable per layer of the laminate, such as in [41].

Design variables related to the choice of the core and skin materials have been progressively introduced in the literature. Choosing the constituent materials for a sandwich structure is intrinsically a discrete problem. One way to solve such a problem is to use continuous parameters to describe the material database, which thus provides the derivatives of the objective and constraint functions. Triantafillou and Gibson [39] gave the closed-form solution for the mass minimization of sandwich beams and plates subjected to strength constraints using the thickness of the core and skin and the core material density as design variables. Wennhage [45] used thickness and density design variables to minimize the mass of a sandwich panel under structural and acoustic requirements using the method of moving asymptotes (MMA) [37]. Derivative-free optimization methods may also be used. Hudson *et al.* [21] used an ant colony algorithm to explore the trade-offs between mass and cost minimization for a rail vehicle floor panel. Wang *et al.* [43] and Leite *et al.* [28] both used genetic algorithms (thereafter GA) to search databases including different kinds of materials, among which some were laminates.

Derivative-free optimization algorithms may also be used for the stacking sequence optimization of the laminate skins. However, these methods are generally penalized by the large number of design evaluations required to reach convergence. Thus, most of the time they were used in combination with a closed-form evaluation of the performance of the structure (e.g. [12,43,21,28,11,14]). But when finite element analyses (FEA) of the solutions are required, the overall computational cost can often be intractable. To face this issue, several authors have proposed to combine GA with approximation techniques and have applied their methods to the optimization of laminated sandwich structures. Kodiyalam *et al.* [26] combined a GA with a linear approximation method to minimize computational cost. The method was applied to minimize the thermally-induced surface distortion of a satellite reflector structure and to minimize the mass of a solar array substrate. Gantovnic *et al.* [15] developed a GA with memory and spline interpolation of the fitness function value to minimize the mass of a sandwich panel under buckling and strength constraints.

The most advanced optimization approaches for composite laminates are multi-step methods. These methods have been developed for large monolithic structures, in particular for variable-stiffness structures [16]. The first attempt at extending the two-step approach to laminated sandwich structures was performed by Balabanov *et al.*

[6]. In the first optimization step, the thickness and macroscopic stiffness distributions of the laminated sandwich composites are optimized using continuous design variables and gradient based optimization. Both the skin thickness and the stiffness are design variables, together with the core material density and its orientation. The macroscopic stiffness of the laminate skin is parametrized using lamination parameters [18]. The layup of the skin is retrieved in a second optimization step using an analytical solution for a specific class of laminates. The method was used to minimize the mass of a sandwich plate under in-plane loading with strength and buckling constraints, using closed-form solutions. Silva and Meddaikar [36] extended the lamination parameters scheme used in the first optimization step for sandwich panel and hybrid laminate design. Catapano and Montemurro [8,9] proposed another two-step strategy, further developed in [31]. During the first optimization step, the polar parametrization is used to describe the macroscopic elastic properties of the laminate skins. The properties of the core material are obtained using a multiscale FE homogenization method. Design variables are related to both the laminate skins and the sizing of the unit cell of the honeycomb core. A GA is used to solve step 1 due to the high non-linearity and non-convexity of the problem. A GA is also used at the second optimization step to retrieve the laminates that match the target properties obtained from step 1.

Only a few studies have focused on the optimization of variable-thickness laminate skins for sandwich structures, mainly because it is mostly relevant for large structures. Velea at al. [41] designed a composite sandwich car body using gradient-based optimization and a multi-step approach. Fan et al. [14] developed a specific genetic algorithm to handle ply drops in the laminate skins.

In the present work, a multi-step optimization strategy is proposed for the design of launcher structures made of laminated sandwich materials. The method is able to deal with thickness variations of the laminate skins obtained by adding or terminating plies. It is applicable to large FE models using shell elements to represent the laminated sandwich composites, in accordance with the usual modeling practice at CNES. Section 2 presents the optimization strategy. The homogenization method for the sandwich composites is detailed in Section 3. Section 4 gives further details about each optimization step and their consistency. Finally an application is presented in Section 5 with the mass minimization of a dual-launch system under stiffness, buckling and strength constraints, submitted to a variety of load cases.

2 Global optimization strategy

The optimization problem at hand can be stated as follows:

$$\min_{\{\boldsymbol{\theta},\mathbf{t_c},\mathbf{t_s}\}} m(\mathbf{t_c},\mathbf{t_s}) \quad \text{subject to:} \begin{cases} g_j(\boldsymbol{\theta},\mathbf{t_c},\mathbf{t_s}) \leq 0 \text{ with } j = 1, \ldots, \text{J} \\ q_l(\boldsymbol{\theta}) \leq 0 \text{ with } l = 1, \ldots, \text{L}, \\ \boldsymbol{\theta} \in \boldsymbol{\Theta} \\ \mathbf{t_c} \in \left[t_c^{min}, t_c^{max}\right]^{n_z} \\ \mathbf{t_s} \in \left[t_s^{min}, t_s^{max}\right]^{n_z} \end{cases}, \tag{1}$$

where m is the mass of the structure. $\mathbf{t_c}$ is the core thickness and $\mathbf{t_s}$ the thickness of the skin. In this work, only sandwich plates that are symmetrical with respect to their mid-plane are considered. As a result, both their skins are assumed identical. They are built from the same elementary layer, with a given material and thickness. Thus, only a single skin thickness variable is required, which is directly related to the number of plies in the skin. The materials of the core and of the elementary layer of the skins are fixed throughout the entire optimization process and thus are not considered as design variables. $\boldsymbol{\theta}$ is the function of ply orientation of the laminate skin. Thus, $\boldsymbol{\theta}$ is a piecewise constant function of z, defined in the thickness of the laminate, with z the out-of-plane coordinate. The ply orientations can take any value within the predefined set $\boldsymbol{\Theta}$.

The design variables $\{\boldsymbol{\theta},\mathbf{t_c},\mathbf{t_s}\}$ can be defined for the whole composite structure, or for each of its sub-regions, so as to define a constant stiffness optimization or a variable stiffness optimization respectively. n_z is the number of sub-regions. The design constraints g_j are related to the mechanical responses of the structure. The constraints q_l correspond to the laminate design guidelines commonly used in the aeronautical industry (e.g. laminate balance, symmetry or 10 % rule [3]).

Figure 1 illustrates the general principle of the proposed optimization strategy. In the first step, the composite material is seen as an equivalent homogenized material. The optimization consists in finding the local stiffness and thickness distributions that minimize the mass of the structure, while satisfying design constraints that most of the time directly derive from the specifications of the structure. The design variables are considered as continuous and taking values in a convex space. As a result, gradient-based optimization algorithms shall be used.

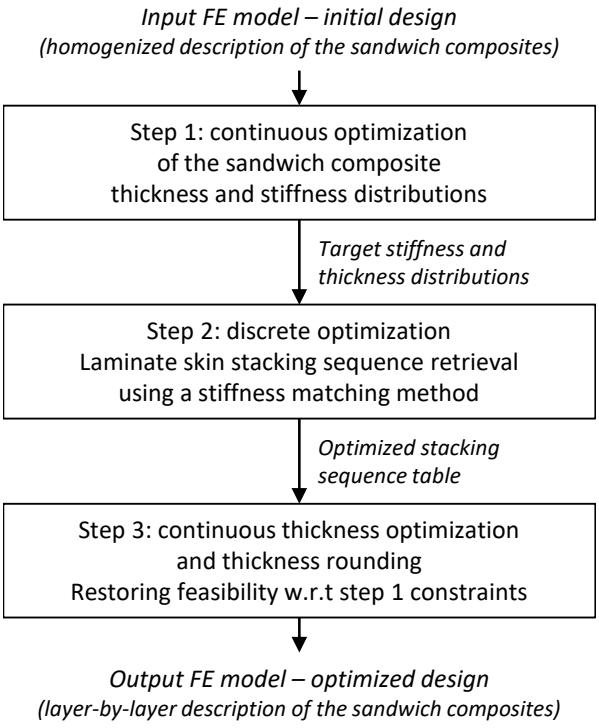

Fig. 1 Workflow of the optimization strategy.

Step 1 optimization problem can then be stated as follows:

$$\min_{\{\mathbf{v},\mathbf{t_c},\mathbf{t_s}\}} m(\mathbf{t_c},\mathbf{t_s}) \quad \text{subject to:} \begin{cases} g_j(\mathbf{v},\mathbf{t_c},\mathbf{t_s}) \le 0 \text{ with } j = 1,\ldots,\mathrm{J} \\ q'_l(\mathbf{v}) \le 0 \text{ with } l = 1,\ldots,\mathrm{L}', \\ \mathbf{v} \in \mathbf{V} \\ \mathbf{t_c} \in \left[t_c^{min}, t_c^{max}\right]^{n_z} \\ \mathbf{t_s} \in \left[t_s^{min}, t_s^{max}\right]^{n_z} \end{cases}, \tag{2}$$

where $\mathbf{v}$ is a vector of continuous design variables used to parametrize the homogenized stiffness of the skin material. The two different sets of parameters most commonly used for that purpose are the polar parameters and the lamination parameters, which are used in this work. The constraints q'_l are a transcription, in terms of lamination parameters, of the subset of the design guidelines q_l that are still applicable to an equivalent homogenized material.

The search for the optimal stacking sequence of the skins is performed in the second step. The objective is to fit the optimal stiffness distribution found in step 1, while taking into account all laminate design guidelines :

$$\min_{\{\boldsymbol{\theta},\mathbf{n}\}} d(\mathbf{S}(\mathbf{v}^*,\mathbf{t_s}^*),\mathbf{S}(\boldsymbol{\theta},\mathbf{n})) \quad \text{subject to:} \begin{cases} q_l(\boldsymbol{\theta}) \le 0 \text{ with } l = 1,\ldots,\mathrm{L}, \\ \boldsymbol{\theta} \in \boldsymbol{\Theta} \\ \mathbf{n} \in [\![n_{min}\,;\, n_{max}]\!]^{n_z} \end{cases}, \tag{3}$$

where $\mathbf{n}$ is the vector of the number of plies, $\mathbf{S}$ represents the laminate homogenized stiffness and $\mathbf{v}^*$ and $\mathbf{t_s}^*$ are the solutions of problem (2). When the structure is divided into several design sub-regions, step 2 corresponds to a laminate blending optimization problem. The blended laminates are described using SSTs, or stacking sequence tables. The SST defines a stacking sequence for each number of plies between n_{max} and n_{min}. These bounds are set with respect to the maximum and minimum thickness in $\mathbf{t_s}^*$, rounded to an integer number of plies. If several independent structures are simultaneously optimized, an independent SST is associated to each structure. Problem (3) is solved using the evolutionary algorithm found in [24] (see section 4.2 for more details).

The discrete and combinatorial optimization in step 2 is based on analytical models with low computational cost – compared to the structural analyses performed during step 1 – which enables using appropriate algorithms (i.e. metaheuristics). However, such analytical models cannot take into account the design constraints g_j based on the mechanical responses of the structure.

Since the minimization of the mass of the structure at step 1 will eventually activate at least one design constraint, it is most likely that the solution returned by step 2 is non feasible with respect to some of the constraints g_j. Hence, a third step is proposed here, in order to restore the feasibility of the solution.

In step 3, the design space is explored in the vicinity of the design found from step 2, to retrieve an acceptable solution. The following optimization problem is considered:

$$\min_{\{\mathbf{t_c},\mathbf{t_s}\}} m(\mathbf{t_c},\mathbf{t_s}) \quad \text{subject to:} \begin{cases} g_j(\mathbf{v},\mathbf{t_c},\mathbf{t_s}) \le 0 \text{ with } j = 1,\ldots,\mathrm{J} \\ \mathbf{v} = f(\boldsymbol{\theta}^*,\mathbf{t_s}) \\ \mathbf{t_s} \in t_p \times [\![min(\mathbf{n}^*) - 1\,;\, max(\mathbf{n}^*) + 1]\!]^{n_z} \\ \mathbf{t_c} \in \left[t_c^{min}, t_c^{max}\right]^{n_z} \end{cases}, \tag{4}$$

with $\mathbf{n}^*$ and $\boldsymbol{\theta}^*$ the solutions of problem (3) and t_p the thickness of the ply.

The step 3 optimization problem is a structural optimization problem, very similar to step 1, since it shares the same objective and constraint functions g_j. Nonetheless, the only design variables handled at step 3 are the thickness of the skin $\mathbf{t_s}$ and the thickness of the core material $\mathbf{t_c}$. The thickness of the skin is considered first as a continuous design variable which is later forced to converge to discrete values corresponding to integer number of plies. Indeed, the purpose of step 3 is solely to add or remove some plies in order to restore feasibility with respect to the optimization constraints g_j, if needed. The optimization performed in step 3 is based on the stacking sequences found in step 2, which satisfy all the laminate design guidelines q_l. Precisely, thanks to the use of SSTs, admissible stacking sequences are known for any num-

ber of plies between $min(\mathbf{n}^*)-1$ and $max(\mathbf{n}^*)+1$. Therefore, based on these stacking sequences, one can build an approximation f of the homogenized material stiffness of the shell element as a function of the number of plies. This approximation function is used to evaluate the skin material properties during optimization (see section 4.3). The thickness of the core material is also considered as a design variable in order to widen the design space and compensate for the possible discrepancy between the laminates obtained at step 2 and the target from step 1. Step 3 returns a final design described, in the case of a sandwich structure, in terms of skin and core thickness distributions, and stacking sequences of the laminate skins. The latter are fully described by the stacking sequence table, closely similar to the draping plans that are used in the industry for manufacturing composite structures.

3 Material stiffness parametrization

Both step 1 and step 3 of the proposed optimization strategy (see Figure 1) make use of a continuous parametrization of the composite sandwich homogenized stiffness.

3.1 First order shear deformation theory

Composite sandwich structures are generally modelled using thick shells. In such a case, the first order shear deformation theory (FSDT) can be used to obtain the general behaviour law of the shell [35]:

$$\begin{Bmatrix} \mathbf{N} \\ \mathbf{M} \\ \mathbf{T} \end{Bmatrix} = \begin{bmatrix} \mathbf{A} & \mathbf{B} & 0 \\ \mathbf{B} & \mathbf{D} & 0 \\ 0 & 0 & \mathbf{F} \end{bmatrix} \begin{Bmatrix} \boldsymbol{\varepsilon}^{\mathbf{0}} \\ \boldsymbol{\kappa} \\ \boldsymbol{\gamma} \end{Bmatrix}. \tag{5}$$

where $\mathbf{N}$, $\mathbf{M}$ et $\mathbf{T}$ are, respectively, the membrane forces, the bending moments and the transverse shear forces, while $\boldsymbol{\varepsilon}^{\mathbf{0}}$, $\boldsymbol{\kappa}$ et $\boldsymbol{\gamma}$ are the in-plane strains, curvatures, and transverse shear strains at the laminate mid-plane. The local stiffness of the material is governed by the set of stiffness tensors $(\mathbf{A},\mathbf{D},\mathbf{F})$, which represent respectively the membrane, bending, and transverse stiffnesses, as well as tensor $\mathbf{B}$, which governs the interactions between membrane and bending effects. When the material is a laminate made out of layers with orthotropic behaviour, the stiffness tensors can be defined as follows :

$$\begin{aligned} \mathrm{A}_{ij} &= \sum_{k=1}^{\mathrm{N}} \mathrm{Q}_{ij}^{(k)}(z_k - z_{k-1}), \\ \mathrm{B}_{ij} &= \frac{1}{2}\sum_{k=1}^{\mathrm{N}} \mathrm{Q}_{ij}^{(k)}(z_k^2 - z_{k-1}^2), \\ \mathrm{D}_{ij} &= \frac{1}{3}\sum_{k=1}^{\mathrm{N}} \mathrm{Q}_{ij}^{(k)}(z_k^3 - z_{k-1}^3), \\ \mathrm{F}_{ij} &= \sum_{k=1}^{\mathrm{N}} \mathrm{C}_{ij}^{(k)}(z_k - z_{k-1}),\ (i,j=4,5). \end{aligned} \tag{6}$$

where the $\mathrm{Q}_{ij}^{(k)}$ terms correspond to the reduced stiffness matrix of the elementary layer, and the $\mathrm{C}_{ij}^{(k)}$ terms correspond to the full 3D stiffness matrix of said layer. In the general case, the core material orientation is not necesarrily aligned with the reference axes of the sandwich plate. As such, the terms C_{ij} are expressed as a function of the transverse shear stiffness moduli G_{13} and G_{23} of the core material as follows:

$$\begin{aligned} \mathrm{C}_{44} &= \mathrm{G}_{23}\cos^2\delta + \mathrm{G}_{13}\sin^2\delta, \\ \mathrm{C}_{45} &= (\mathrm{G}_{13} - \mathrm{G}_{23})\sin\delta\cos\delta, \\ \mathrm{C}_{55} &= \mathrm{G}_{23}\sin^2\delta + \mathrm{G}_{13}\cos^2\delta, \end{aligned} \tag{7}$$

with δ the rotation angle from the plate reference axes to the material orthotropy axes, in the plane of the plate.

3.2 Laminate face sheets

The lamination parameters (thereafter LP) bring a condensed and practical representation of the stiffness matrices $\mathbf{A},\mathbf{B}$ and $\mathbf{D}$ of composite laminates [40]. This representation connects a set of four continuous dimensionless parameters to each of those matrices. Each one of these parameters is defined as a trigonometrical sum of the material orientation $\theta(z)$ over the thickness of the plate:

$$\begin{aligned} \mathrm{V}^{\mathrm{A}}_{[1,2,3,4]} &= \int_{-1/2}^{1/2} [\cos 2\theta(z), \sin 2\theta(z), \cos 4\theta(z), \sin 4\theta(z)]\, d\bar{z}, \\ \mathrm{V}^{\mathrm{B}}_{[1,2,3,4]} &= 4\int_{-1/2}^{1/2} \bar{z}[\cos 2\theta(z), \sin 2\theta(z), \cos 4\theta(z), \sin 4\theta(z)]\, d\bar{z}, \\ \mathrm{V}^{\mathrm{D}}_{[1,2,3,4]} &= 12\int_{-1/2}^{1/2} \bar{z}^2[\cos 2\theta(z), \sin 2\theta(z), \cos 4\theta(z), \sin 4\theta(z)]\, d\bar{z}, \end{aligned} \tag{8}$$

where $\bar{z}$ is the normalized out-of-plane dimension, i.e. $\bar{z} = z/t_s$.

Equation 9 shows that the total macroscopic stiffness matrix of the laminate — disregarding transverse shear effects — is a linear function of the LP, of the total thickness t of the laminate, and of the elementary matrices $\mathbf{\Gamma}_{i=0,\ldots,4}$

which are characteristic of the elementary ply and as such are considered constant during the optimization process.

$$\begin{aligned}\mathbf{A} &= t_s\left(\mathbf{\Gamma}_0+\mathbf{\Gamma}_1\mathrm{V}_1^{\mathrm{A}}+\mathbf{\Gamma}_2\mathrm{V}_2^{\mathrm{A}}+\mathbf{\Gamma}_3\mathrm{V}_3^{\mathrm{A}}+\mathbf{\Gamma}_4\mathrm{V}_4^{\mathrm{A}}\right),\\ \mathbf{B} &= \frac{t_s^2}{2}\left(\mathbf{\Gamma}_0+\mathbf{\Gamma}_1\mathrm{V}_1^{\mathrm{B}}+\mathbf{\Gamma}_2\mathrm{V}_2^{\mathrm{B}}+\mathbf{\Gamma}_3\mathrm{V}_3^{\mathrm{B}}+\mathbf{\Gamma}_4\mathrm{V}_4^{\mathrm{B}}\right),\\ \mathbf{D} &= \frac{t_s^3}{12}\left(\mathbf{\Gamma}_0+\mathbf{\Gamma}_1\mathrm{V}_1^{\mathrm{D}}+\mathbf{\Gamma}_2\mathrm{V}_2^{\mathrm{D}}+\mathbf{\Gamma}_3\mathrm{V}_3^{\mathrm{D}}+\mathbf{\Gamma}_4\mathrm{V}_4^{\mathrm{D}}\right).\end{aligned} \tag{9}$$

Thus, this representation allows to determine the full mechanical response of a laminated plate using 12 lamination parameters and the thickness t_s, irrespective of the number of plies. That is 13 variables as opposed to the 18 components of the **A**, **B** and **D** tensors in the general case. On top of that, these 13 variables vary continuously, and as such are suitable for use in a gradient-based algorithm, contrary to the discrete orientations of the layers, or the number of plies.

This representation runs under a few limiting assumptions. First, the lamination parameters are restricted to the case of composite laminates, as opposed to a general anisotropic material. Second, they can only be used to parametrize the reduced stiffness matrices of the material, and thus are not suitable for use in compliance-based optimization problems. Third, the direction of the axes of orthotropy of the homogenized material is fixed and is not considered as an optimization variable. However, such an additional design variable can easily be introduced in the lamination parameters framework (see [19]). Whenever any of the previous three limitations come into play, the more generally applicable polar representation can be used with the same purpose as the lamination parameters. Finally, it is assumed that the laminate is made out of identical plies (same material properties). Thus, as such, the representation used here may not be used for hybrid laminates (two or more different kinds of layers). An extension of the lamination parameters scheme for hybrid laminates is presented in [36].

3.3 Symmetrical sandwich plates with laminate skins

The present work focuses on the case of symmetrical sandwich plates, with a thick core surrounded by two mirrored laminated sheets called the skins. In this case, one may apply equation 6 by considering the core as an additional layer with its own material. Under this premise, relation 5 still applies, and the components of the four homogenized stiffness tensors are now given by Eq. 10 [7]:

$$\begin{aligned}\mathrm{A}_{ij} &= 2\mathrm{A}_{ij}^{(s)} + t_c\mathrm{Q}_{ij}^{(c)},\\ \mathrm{B}_{ij} &= 0,\\ \mathrm{D}_{ij} &= \frac{1}{2}\mathrm{A}_{ij}^{(s)}\left[(t_s+t_c)^2+\frac{t_s^2}{3}\right]+\mathrm{Q}_{ij}^{(c)}\frac{t_c^3}{12},\\ \mathrm{F}_{ij} &= 2\mathrm{F}_{ij}^{(s)} + t_c\mathrm{G}_{ij}^{(c)},\end{aligned} \tag{10}$$

where $\mathrm{A}_{ij}^{(s)}$ are the components of the membrane stiffness of a single skin (see equation 5), $\mathrm{Q}_{ij}^{(c)}$ are the components of the reduced stiffness matrix of the core material, $\mathrm{G}_{ij}^{(c)}$ are the transverse shear moduli of the core material, and t_c is the core *total* thickness.

3.4 Transverse shear stiffness

The transverse shear stiffness **F** of the sandwich plate defined in equation 6 can be parametrized using two in-plane lamination parameters:

$$\mathbf{F} = t\left(\mathbf{\Lambda}_0+\mathbf{\Lambda}_1\mathrm{V}_1^{\mathrm{A}}+\mathbf{\Lambda}_2\mathrm{V}_2^{\mathrm{A}}\right), \tag{11}$$

where the elementary matrices $\mathbf{\Lambda}_{i=0\ldots2}$ are computed from the transverse shear stiffness of the skin material:

$$\begin{aligned}\mathbf{\Lambda}_0 &= \frac{1}{2}(\mathrm{G}_{13}+\mathrm{G}_{23})\begin{bmatrix}1&0\\0&1\end{bmatrix},\\ \mathbf{\Lambda}_1 &= \frac{1}{2}(\mathrm{G}_{23}-\mathrm{G}_{13})\begin{bmatrix}1&0\\0&-1\end{bmatrix},\\ \mathbf{\Lambda}_2 &= \frac{1}{2}(\mathrm{G}_{13}-\mathrm{G}_{23})\begin{bmatrix}0&1\\1&0\end{bmatrix}.\end{aligned} \tag{12}$$

It is thus possible to parametrize the transverse shear stiffness of the sandwich composites in equation 10 with two membrane lamination parameters only.

In practice, commercial FE tools do not use the definition given in equation 6 for the transverse shear stiffness. As a matter of fact, the FSDT gives a simplistic approximate of **F** with constant shear stresses through the thickness of the ply that do not satisfy the local equilibrium. Moreover, the transverse shear stress resulting from equation 5 is discontinuous between the layers and is not null on the top and bottom surface of the laminate, which should be the case in the absence of applied tangential forces. Several modifications of the expression of **F** have been proposed in the past decades (for a deeper insight on the topic, see [35]). Corrective factors k_{ij} thus appear in the definition of transverse shear stiffness, such that:

$$\begin{Bmatrix}\mathrm{T}_y\\ \mathrm{T}_x\end{Bmatrix} = \begin{bmatrix}\mathrm{H}_{44}&\mathrm{H}_{45}\\ \mathrm{H}_{45}&\mathrm{H}_{55}\end{bmatrix}\begin{Bmatrix}\gamma_{yz}\\ \gamma_{xz}\end{Bmatrix}, \tag{13}$$

where:

$$\mathrm{H}_{ij} = k_{ij}\mathrm{F}_{ij}, \text{ with } i,j = 4,5. \tag{14}$$

Weckner and Balabanov [44] studied the influence of the shear correction factors on the buckling of a thick sandwich plate, showing significant influence.

The determination of these corrective factors is complex and varies across different commercial FE softwares. For instance, Nastran reference manual [2] presents a transverse shear theory in which the corrected homogenized transverse shear stiffness H_{ij} is not related to the transverse shear stiffness F_{ij} of the FSDT using equation 14. In every case though, one may observe a strong dependence of the factors H_{ij} on the stacking sequence of the laminates and, in the case of sandwich materials, on the ratio between the core thickness and the skin thickness. The dependence to the ply stacking order is significant for laminates, but decreases with the ratio t_s/t_c for symmetrical sandwich plates.

Such dependence is difficult to take into account in the optimization. On one hand, our homogenization scheme must mimic the homogenization procedure of the FE software in order to produce consistent results. On the other hand, an adequate parametrization of **H** is needed. Equations 9, 10 and 11 show that in the framework of the FSDT, the elastic behaviour of the sandwich material can fully be parametrized using only six variables, namely V_1^A, V_2^A, V_3^A, V_4^A, t_s and t_c. But equation 14 also means that additional parameters are required to capture the influence of the stacking order on the transverse shear stiffness correction factors.

In this work, a neural network (NN) is used to approximate the components of the tensor **H**, using nine variables for symmetrical sandwich composite plates: four membrane lamination parameters of the skin, four bending lamination parameters of the skin and the core-to-skin thickness ratio. A database of 5480 preliminary analyses is built using MSC Nastran homogenization module. The design space is sampled using a set of 548 symmetrical 8-ply laminates made of two ply orientations θ_1 and θ_2 taking values in the set $\{-75,60,\ldots,75,90\}$. These laminates are then combined with a core with a thickness ratio t_c/t_s in the set $\{0.5,1,2,3,4,5,6,8,10,20\}$. Half of the database is used to train the neural network, the other half being used for validation. The metamodel is built for a fixed couple of materials for the skin elementary layer and for the core.

Figure 2 shows the dispersion graph of H_{44} based on all 5480 points. The material properties used here correspond to the application case detailed in section 5. The error between the approximated values of H_{44} and the reference data is less than 10%, in absolute value, for more than 99% of the points, with a 12% maximal error. Similar approximation quality is obtained for H_{55} and H_{45}. The values of H_{44} computed with Altair OptiStruct (OS) homogenization module are given in the figure for comparison. It is interesting to note that both FE code are in rather good

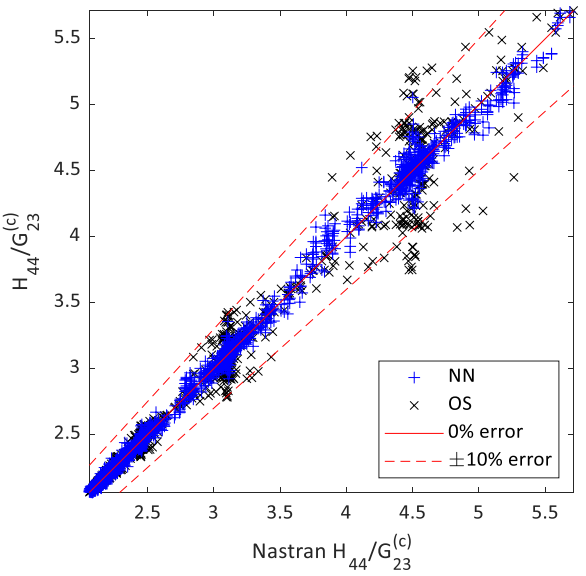

Fig. 2 Dispersion graph of the corrected transverse shear stiffness term F_{44} (NN: Neural Network approximation, OS: OptiStruct homogenization module).

agreement, even if some discrepancies can be observed. With 98% of the points showing an error inferior to 10% with respect to the OptiStruct reference, we consider in the following that the metamodel is consistent with both FE software. Note that the mean error in absolute value between F_{44} and H_{44} is about 560% which justifies the use of the metamodel, rather than the classical formulation (eq. 12).

4 From stiffness-based to ply-by-ply description

The overall performance of the strategy pictured in Figure 1 strongly depends on the consistency between the stiffness-based representation of the sandwich composite plate and its ply-by-ply representation. This section explains how, step by step, the accuracy of the mechanical modeling is improved as more information gets available about the laminates.

4.1 Step 1: feasible domain of the lamination parameters

The link between step 1 and the subsequent steps lies in a set of constraints imposed on the lamination parameters. These constraints are twofold. A first set of constraints aims at defining the feasible region **V** for the lamination parameters **v** (see problem (2)), *i.e.* the region of the design space that does correspond to actual laminates. The feasible domain for the four in-plane lamination parameters is de-

fined by [19]:

$$\begin{aligned} &2(\mathrm{V}_1^{\mathrm{A}})^2(1-\mathrm{V}_3^{\mathrm{A}})+2(\mathrm{V}_2^{\mathrm{A}})^2(1+\mathrm{V}_2^{\mathrm{A}})+(\mathrm{V}_3^{\mathrm{A}})^2+(\mathrm{V}_4^{\mathrm{A}})^2\ldots \\ &\qquad\qquad \ldots-4\mathrm{V}_1^{\mathrm{A}}\mathrm{V}_2^{\mathrm{A}}\mathrm{V}_4^{\mathrm{A}}\leqslant 1, \\ &(\mathrm{V}_1^{\mathrm{A}})^2+(\mathrm{V}_2^{\mathrm{A}})^2\leqslant 1, \\ &-1\leq \mathrm{V}_i^{\mathrm{A}}\leqslant 1\ (i=1,\ldots,4). \end{aligned} \tag{15}$$

Taking into account the approximation of the transverse shear stiffness presented in section 3.4 in the optimization requires introducing the four bending lamination parameters as additional variables for each optimization region of the structural model. The feasible space for the coupled in-plane and bending parameters can be described using the set of inequalities proposed in [13]. However, in the homogenization scheme described in section 3 the bending lamination parameters only influence the transverse shear stiffness of the sandwich material, which, in turn, only has a second order influence on the constraints of the optimization problem described in section 2. Hence, adding the bending parameters as additional design variables present a risk of hampering the optimization in step 1. Instead, we propose to use in step 1 the following simplifying assumption: $\mathrm{V}_i^{\mathrm{D}}=\mathrm{V}_i^{\mathrm{A}}$ $(i=1,\ldots,4)$. By doing so, the accuracy of the approximation of the transverse shear stiffness using the neural network devised in section 3.4 is slightly reduced. The proportion of the validation database with an absolute error less than 10%, with respect to reference data, is 96%, while the maximal error increases to 27%, which is deemed acceptable. Overall, this approach provides a reasonable balance between the accuracy of the approximation of the transverse shear stiffness of the plate, and the performance of the first optimization step. The design variables used at step 1 are the membrane lamination parameters $\mathrm{V}_i^{\mathrm{A}}$ $(i=1,\ldots,4)$, the skin thickness t_s and the core thickness t_c.

A second set of constraints q_l' incorporates some of the laminate design guidelines q_l (see problem (1)) into step 1. These constraints can help to improve the consistency between step 1 and the subsequent optimization steps. Examples of such guidelines are:

- Searching for balanced laminates, which are orthotropic in membrane with $\mathrm{V}_2^{\mathrm{A}}=\mathrm{V}_4^{\mathrm{A}}=0$. Let us note however that balancing the stacking sequence is only a sufficient condition for in-plane orthotropy, and reduces the design space of the stacking sequences. It is however common industrial practice to use such laminates and thus this guideline is widely enforced in the literature.
- The 10%-rule, which can be stated, in a stiffness-based description, as a minimal in-plane stiffness requirement in all directions [3].
- In case of variable thickness optimization, blending design guidelines may be taken into account using a set of blending constraints. Such constraints have been expressed in the lamination parameter space [29] as well as using the polar representation [32,34].

4.2 Step 2: stacking sequence tables

Step 2 is based on a ply-by-ply representation of the sandwich material and its laminate skins. The discrete optimization step is based on an evolutionary algorithm specialized for stacking sequence tables [24]. The notion of a stacking sequence table (thereafter SST) comes from current industrial manufacturing practice, is easily interpreted in terms of the draping plan of a part and simplifies the transition between design and manufacturing. Additionally, a SST is a very general formulation of the problem, since the ply orientations as well as the positions of the ply-drops within the stack are all design variables. Moreover, it has the advantage that many industrial design guidelines can be conveniently enforced using such a representation.

A SST assigns a given stacking sequence to any number of plies within a given interval $[\![n_{min};n_{max}]\!]$. Hence, for a known distribution of thickness over the structure, the SST gives the stacking sequence corresponding to the number of plies assigned to each zone. The entire stacking sequence information of a blended panel is encoded through a SST using a three chromosome genotype, hence making it possible to optimize the structure using a minimal number of design variables.

- The first chromosome $\mathbf{X}_s$ represents the stacking sequence of the thickest laminate in the SST.
- The second chromosome $\mathbf{X}_i$ represents the order of insertion of the plies within the laminate.
- The third chromosome $\mathbf{X}_n$ represents the number of plies in each region of the structure.

The first two chromosomes are integer vectors of length n_{max}. They completely define the SST. Figure 3 illustrates the SST defined by $\mathbf{X}_s$ = [45 90 75 90 -75 -45 0 0 -45 -75 90 75 90 45] and $\mathbf{X}_i$ = [0 5 4 0 1 0 0 0 0 2 0 3 6 0]. A 0 value in $\mathbf{X}_i$ indicates that the ply is always present in the table, from the thinnest to the thickest laminate. The third chromosome, $\mathbf{X}_n$, is an integer vector of length n_z, the number of regions over the structure. In step 2, $\mathbf{X}_n$ is obtained by rounding the optimal thickness distribution $\mathbf{t_s}^*$ from step 1. Rounding can be performed by following a fixed rule (e.g. rounding to the nearest integer), in which case $\mathbf{X}_n$ is fixed. Alternatively, rounding can be considered as part of the optimization problem itself and the components of $\mathbf{X}_n$ may vary within a user-defined integer interval centered on the continuous optimum $\mathbf{t_s}^*$.

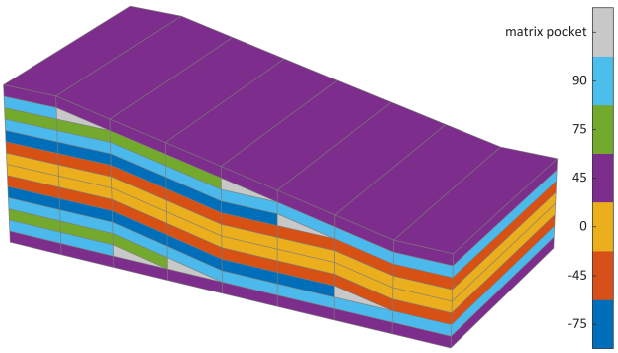

Fig. 3 Example of stacking sequence table.

Step 2 optimization problem (see problem (3)) consists in finding the SSTs that minimize the distance between the target stiffness distribution $S(\mathbf{v}^*, \mathbf{t_s}^*)$ from step 1 and the distribution corresponding to the discrete design. If several independent structures are simultaneously optimized, an independent SST is associated to each structure. In the case of sandwich plates, with a fixed core thickness t_c^*, the stiffness distribution S is completely defined by the thickness and the stiffness properties of the skins. In this work, the symmetrized Kullback-Leibler (KL) [30, 23] divergence is used to measure the difference between two symmetric positive-definite stiffness tensors $\mathbf{A}_1$ and $\mathbf{A}_2$:

$$d(\mathbf{A}_1, \mathbf{A}_2) = tr(\mathbf{A}_1^{-1}\mathbf{A}_2 + \mathbf{A}_1\mathbf{A}_2^{-1} - 2\mathbf{I}). \tag{16}$$

The distances are computed for each region of the structure and aggregated through a weighted sum. The weight of each zone is the ratio of its area over the total area of the structure.

4.3 Step 3: continuous representation of a SST

The best SST obtained at the end of step 2 contains all the information needed to fully describe the discrete evolution of the homogenized stiffness as a function of the number of plies in the skin. Thus, the relation between the number of plies and the homogenized in-plane stiffness of the skin is completely defined. This relation can easily be extended to continuous thickness variations. Indeed, each newly added ply can be progressively introduced in the laminate by increasing its thickness from zero to the full ply thickness. For a given SST, this enables computing all the skin laminate stiffness properties as a function of the laminate thickness t_s, and in turn, the equivalent sandwich plate properties. This SST representation is core to step 3, since it allows to match directly the number of layers of the skin, which is one of the design variables in step 3 (see eq. 4), to a given stacking sequence provided by the SST. This operation does not require an additional search for the orientation of the added layer, or for the position of the layer to be removed, and is thus very efficient. Figure 4 shows the evolution of the membrane and bending lamination parameters with respect to the laminate thickness for the SST depicted in figure 3.

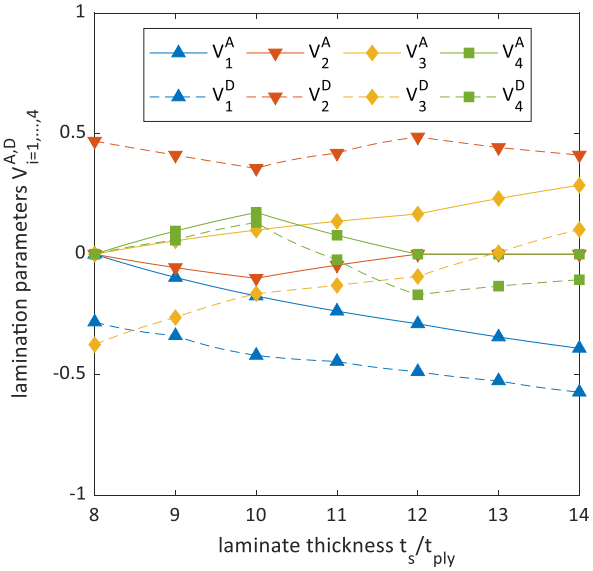

Fig. 4 Continuous representation of the SST shown in figure 3. Evolution of the membrane and bending lamination parameters as a function of the local laminate thickness.

The transverse shear stiffness of the sandwich composite can also be computed using the neural network approximation presented in section 3.4. However, contrary to step 1, the exact values for all the membrane and bending lamination parameters of the skin are known, since the stacking sequences are described throught the SST. Thus, the accuracy of the approximation of the transverse shear stiffness is improved with respect to step 1 (see section 4.1). Finally, at the end of step 3, the sandwich plate is described layer by layer, and it is this description that is used to evaluate the final design performance. At the end of step 3, the only possible discrepancy between the homogenized description of the material and its explicit description (using a single thick shell element) comes from the approximation of the transverse shear stiffness with the metamodel.

4.4 Enforcing strength constraints

Failure criteria for composite laminates are usually defined at ply scale. Thus, incorporating a strength constraint into the lamination parameter optimization process is not straightforward. Ijsselumuiden *et al.* [22] derived the equations of a conservative first-ply failure envelope based on the Tsaï-Wu failure criterion. The failure envelope is formulated on the macroscopic in-plane strains. The failure

safe region corresponds to the region in strain space that is safe regardless of the ply angle. Thus, the failure envelope can be used with an homogenized description of the laminates. Alternatively, Catapano *et al.* have derived the relationship between the polar parameters of the stiffness and strength matrices of the laminate, for a variety of strength criteria [10].

Conservative failure envelopes can be computed, either numerically or as closed-form solutions of the composite failure criteria. Depending on the chosen failure criterion, the equations of the conservative envelope can be difficult to obtain, and subsequently difficult to use for a strength-related optimization constraint. A more pragmatic method consists in sampling the ply orientations and computing the corresponding in-plane failure envelopes. The conservative failure envelope then corresponds to the boundary of the intersection of all the failure safe regions obtained this way. This conservative envelope can then be approximated using an ellipsoid. Either the maximum volume inscribed ellipsoid or the minimum volume enclosing ellipsoid can be chosen, depending on the desired level of conservativeness. It is then the equation of the ellipsoid that is used to define the optimization constraint. Thus, the strength constraint can be expressed as follows:

$$(\boldsymbol{\varepsilon}-\mathbf{c})^{\mathrm{T}}\Xi(\boldsymbol{\varepsilon}-\mathbf{c})\leq 1, \tag{17}$$

where $\boldsymbol{\varepsilon}$ corresponds to the macroscopic strains of the laminate. Ξ is the matrix of the ellipsoid and $\mathbf{c}$ its centre. In order to take into account the bending of the structure, the failure criteria has to be evaluated on both outer surfaces of the laminates, where the in-plane strains are the highest.

In section 5, a conservative failure envelope based on the modified Tsaï-Hill failure criterion [25] is used. At ply scale, in the material axes, this criterion can be expressed as:

$$\left(\frac{\sigma_{11}}{X^*}\right)^2-\frac{\sigma_{11}\sigma_{22}}{X_tX_c}+\left(\frac{\sigma_{22}}{Y^*}\right)^2+\left(\frac{\tau_{12}}{S^*}\right)^2\leq 1, \tag{18}$$

where X^* (resp. Y^*) has to be substituted either by the longitudinal tensile strength X_t or compressive strength X_c (resp. Y_t or Y_c in the transverse direction) , depending on the sign of the associated stress component σ_{11} (resp. σ_{22}). S^* is the shear strength of the ply and τ_{12} the shear stress. Figure 5 shows the conservative failure envelope computed for the Tsaï-Wu failure criterion using the method found in [22], along with the conservative failure envelop computed for the modified Tsaï-Hill failure criterion using the method described in this section. It is interesting to note that the conservative failure envelop inherits some features of the criterion on which it is based. Here, the conservative envelop of the Tsaï-Wu criterion is much less conservative than the Tsaï-Hill failure criterion in biaxial compression, which is a well-known limitation of the Tsaï-Wu

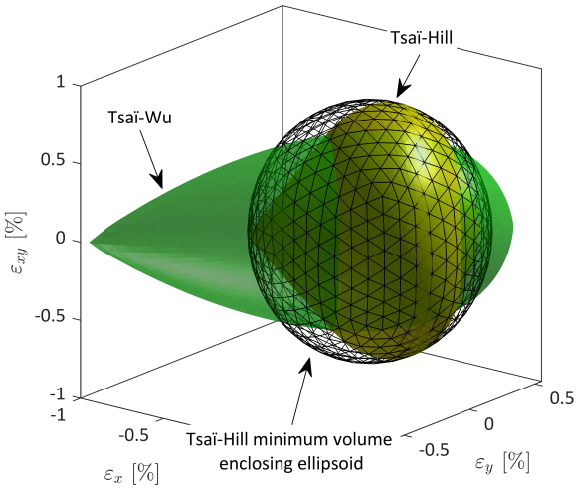

Fig. 5 Conservative failure envelops computed for the Tsaï-Wu and the Tsaï-Hill failure criteria. Wire frame view of the minimum volume enclosing ellipsoid of the Tsaï-Hill conservative envelop.

criterion. The minimum volume enclosing ellipsoid of the modified Tsaï-Hill failure envelope – which is used to define the strength constraints in section 5 – is also shown in the figure.

Failure of a sandwich composite does not come down to the in-plane failure of the facesheet laminates. Sandwich panels can fail through a large variety of mechanisms, including crushing of the core, shear failure of the core, and instabilities such as shear crimping, face sheet wrinkling, or intra-cell dimpling [1,42]. These phenomena stem from complex interactions between the core and the skins. As such, they depend on the nature of the core and skin material [38,33]. The present study focuses on the global design of the structure. The sandwich laminates are modeled using thick shell elements, which are not well suited for the accurate evaluation of the sandwich local failure phenomena. Given that, most of the time, aerospace structural designs are stiffness dominated rather than strength dominated, we choose to ignore all the specific sandwich failure modes during the optimization, and only take face sheet failure into account. However, shear crimping, face sheet wrinkling, and intra-cell dimpling will be reviewed on the final design of the structure, using classical engineering criteria devised for the rapid sizing of sandwich structures.

5 Optimization of a generic Dual-Launch System

The case study is derived from a typical spatial structure, the Ariane 5 Dual-Launch System (SYLDA). Figure 6 shows a general view of the model of the structure. The test case has the dimensions of the real structure, with a central cylinder of approximately 5 m long and 4.5 m in diame-

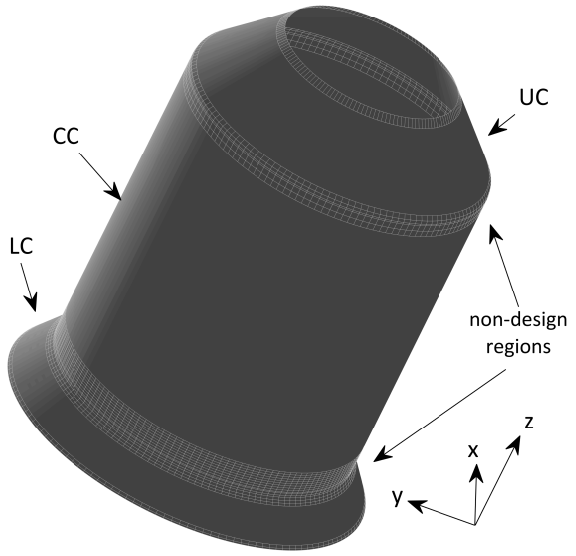

Fig. 6 General view of the test case.

ter. The model is divided into three sections, namely the lower cone (thereafter LC), the central cylinder (CC) and the upper cone (UC). Each of these substructures is made of a sandwich composite material. They are manufactured separately and assembled to form the final part using hybrid composite/metal flanges that are not optimized in this work.

In the following, the proposed optimization method is applied to a change of configuration of the SYLDA. The composite lay-ups of the reference design, used as the starting point of the optimization, correspond to a shorter version of the SYLDA structure. The purpose is to design and optimize a new version of the SYLDA, corresponding to the geometry shown in Figure 6, considering the specifications detailed in the following section. Note that, in the framework of this paper, we do not expect to mimic the whole design process of a large and complex part like the SYLDA. The potential gains in terms of mass can not be directly interpreted as gains that will be achieved on the real structure, but it is still relevant to show that the proposed strategy was able to produce such gains.

Each substructure in the reference design is made of a constant stiffness sandwich composite. In the following, m_0 is mass of the reference design, $t^0_{s(\mathrm{LC})}$ is the thickness of the skin of the lower cone and t^0_c is the thickness of the core material which is the same in the three substructures, with $t^0_c / t^0_{s(\mathrm{LC})} \approx 19$. The length of the structure is aligned with the z-axis. The 0° material orientation is defined by the projection of the z-axis on the surface of the shell elements. The model provided by CNES has about 82,000 degrees of freedom.

The optimization strategy described in Figure 1 has been implemented as an interactive optimization tool using Python. The Python tool can call either MSC Nastran or Altair OptiStruct for step 1 and step 3 optimizations, through text files. The results presented in the following are obtained using OptiStruct. Step 2 calls for an evolutionary algorithm implemented in Matlab. All data transfer and input and output files preparation and writing are fully automated. Between each step, the user can check the results from the previous optimization step and decide whether to continue to the next step or repeat the previous optimization with modified parameters.

5.1 Formulation of the optimization problem

The objective of the overall design problem is to minimize the weight of the structure while satisfying:

- Global stiffness constraints.
- Buckling constraints.
- Strength constraints in the composite skins.

Seven load cases are considered in total , out of which three are elementary unit load cases used to evaluate the global stiffness of the structure. Two other cases correspond to the take-off sequence of the Ariane 5 launcher, where the SYLDA structure will withstand the acceleration and then deceleration of the launcher. The final two load cases correspond to a situation where the launcher experiences a major gust of wind during flight, in two different directions.

The global stiffness constraint is evaluated through the three unit load cases (axial load along z-axis F_z, shearing load along y-axis F_y and bending moment about the x-axis M_x). The structure is clamped at its lower end. Loads and moment are applied at a reference node located at the top of the structure, along its central axis, and transferred to the top of the upper cone using rigid body elements. The corresponding displacements are monitored at the reference node and used to infer a global stiffness matrix. The stiffness constraints themselves are bounding conditions on three components of this matrix, as follows:

$$\begin{aligned} &\mathrm{K}^{min}_{\mathrm{F}_z} \leq \mathrm{K}_{\mathrm{F}_z} \leq \mathrm{K}^{max}_{\mathrm{F}_z}, \\ &\mathrm{K}^{min}_{\mathrm{F}_y} \leq \mathrm{K}_{\mathrm{F}_y} \leq \mathrm{K}^{max}_{\mathrm{F}_y}, \\ &\mathrm{K}^{min}_{\mathrm{M}_x} \leq \mathrm{K}_{\mathrm{M}_x}. \end{aligned} \tag{19}$$

where $\mathrm{K}_{\mathrm{F}_z}$ is an axial stiffness term, $\mathrm{K}_{\mathrm{F}_y}$ a transverse stiffness term and $\mathrm{K}_{\mathrm{M}_x}$ is a bending stiffness term. Note that the reference solution does not satisfy this set of global stiffness constraints.

The four load cases related to the flight of the launcher are introduced through super elements, located on the lower and upper ends of the SYLDA, that represent the global stiffness of the whole launcher structure and payload. Among

these four load cases, two may generate buckling. Considering that for an axially-compressed thin elastic cylindrical shell made of an isotropic material, the linearised buckling equations lead to a critical load that is independent from the length of the cylinder [27], it is assumed here that the reference design inherits satisfying buckling behaviour from the original configuration. Thus, the buckling load factors are constrained to be higher or equal to those of the reference design. In practice, for each load case, the first twenty buckling modes are constrained to take into account mode switching during the optimization. Finally, a strength criterion is applied to the face sheet laminates, using the macroscopic strain envelope discussed in section 4.4.

All things considered, the optimization problem of the SYLDA structure is stated as follows:

$$\min_{\{\boldsymbol{\theta},\mathbf{t_c},\mathbf{t_s}\}} m(\mathbf{t_c},\mathbf{t_s})$$
$$\text{subject to: } \begin{cases} \mathrm{K}_{\mathrm{F}_z}^{min} \le \mathrm{K}_{\mathrm{F}_z}(\boldsymbol{\theta},\mathbf{t_c},\mathbf{t_s}) \le \mathrm{K}_{\mathrm{F}_z}^{max}, \\ \mathrm{K}_{\mathrm{F}_y}^{min} \le \mathrm{K}_{\mathrm{F}_y}(\boldsymbol{\theta},\mathbf{t_c},\mathbf{t_s}) \le \mathrm{K}_{\mathrm{F}_y}^{max}, \\ \mathrm{K}_{\mathrm{M}_x}^{min} \le \mathrm{K}_{\mathrm{M}_x}(\boldsymbol{\theta},\mathbf{t_c},\mathbf{t_s}) \\ \lambda_i^{(1)} \ge \lambda_0^{(1)}, \text{ with } i = 1,\dots,20 \\ \lambda_i^{(2)} \ge \lambda_0^{(2)}, \text{ with } i = 1,\dots,20 \\ (\boldsymbol{\varepsilon}-\mathbf{c})^{\mathrm{T}}\boldsymbol{\Xi}(\boldsymbol{\varepsilon}-\mathbf{c}) \le 1 \\ q_l(\boldsymbol{\theta}) \le 0 \text{ with } l = 1, \dots, \mathrm{L}, \\ \boldsymbol{\theta} \in \boldsymbol{\Theta} \\ \mathbf{t_c} \in \left[t_c^{min}, t_c^{max}\right]^{n_z} \\ \mathbf{t_s} \in \left[t_s^{min}, t_s^{max}\right]^{n_z} \end{cases}, \tag{20}$$

where $\lambda_i^{(j)}$ is the buckling factor of the i-th buckling mode for load case j and $\lambda_0^{(j)}$ is the critical buckling factor of the reference solution.

5.2 Constant-stiffness optimization

Each substructure is assigned a single set of design variables, *i.e.* each substructure is made of a uniform sandwich composite ($n_z = 3$). Taking into account this design choice, step 1 optimization has 18 design variables, namely, for each substructure, the four in-plane lamination parameters of the skin $\mathrm{V}_1^{\mathrm{A}}$, $\mathrm{V}_2^{\mathrm{A}}$, $\mathrm{V}_3^{\mathrm{A}}$, $\mathrm{V}_4^{\mathrm{A}}$, the skin thickness t_s and the core thickness t_c.

It is interesting to compare the optimal design obtained when taking into account the stiffness constraints only (see figure 7), the buckling constraints only (see figure 8), and both constraints simultaneously, as the optimizations converge towards very different designs. In the stiffness-constrained case, the core thickness is reduced in every substructure, since the structural global stiffness is mostly driven by the membrane behaviour of the skins. In the buckling-constrained case, the influence of the core thickness is much more significant since buckling is driven by the bending behaviour of the sandwich composites. Thus the skin thicknesses are lower than in the stiffness-constrained case, while the core thicknesses are much higher. The total mass reduction is about 12.2% in the stiffness-constrained case and 18.5% in the buckling-constrained case.

Step 1 optimization with both stiffness and strength constraints is performed using the multi-model optimization feature of OptiStruct. Figure 9 presents the evolution of mass and thickness. The optimal design combines features of the optimal solution of the stiffness-constrained case, with thick skins, and of the buckling-constrained case, with thick cores. The optimal design is thus heavier than both previous solutions. The total mass reduction is about 5.0% with respect to the reference mass m_0. Figure 10 shows the anisotropy shapes of the skins in each substructure, and for each solution. It shows that the stiffness properties of the skins in the optimal design with all constraints enforced are closer to that of the stiffness-constrained case than that of the buckling-constrained case.

At step 2, each substructure is represented by a SST. The SST is innately a representation of variable thickness laminates, thus it is not the most efficient representation of the solution for constant stiffness matching. Nonetheless, the results obtained turned out to be acceptable, as it is shown in the following. The ply orientations vary by a 5° step. Membrane orthotropy of the laminates is required. Note that the principal orthotropy direction is not a design variable in this work. Based on the symmetries of the problem at hand, it is assumed that the optimal orthotropy direction will be aligned with the longitudinal axis of the structure, i.e. the reference frame of the laminates. In that case, the design guideline on the balance of the skin laminates provides a sufficient condition to achieve membrane orthotropy and as such was enforced at step 2, in spite of the loss of optimality that may result from it, as discussed in section 4.1. However, let us note that in the SST representation, this is introduced as a "soft" constraint, since adding or removing a single ply will necessarily break the balance of the stacking sequence, but is still allowed here. The influence on the overall behaviour of the sandwich plate is expected to be small. No guideline on the symmetry of the laminates was enforced. The evolutionary algorithm was run 10 times using 100 generations of 30 individuals each and the best design out of the 10 runs was selected for step 3. Since no structural computation is done at step 2, the overall computational cost is negligible, which allows for a large number of evaluations.

Step 3 makes use of the SST from step 2 to parametrize the link between the skin thickness and the skin stiffness. The discrete variable optimization feature provided by OptiStruct is used to round the skin thickness to actual ply numbers at the end of step 3. The step-by-step results of the three optimizations are summarized in Table 1. Step 2

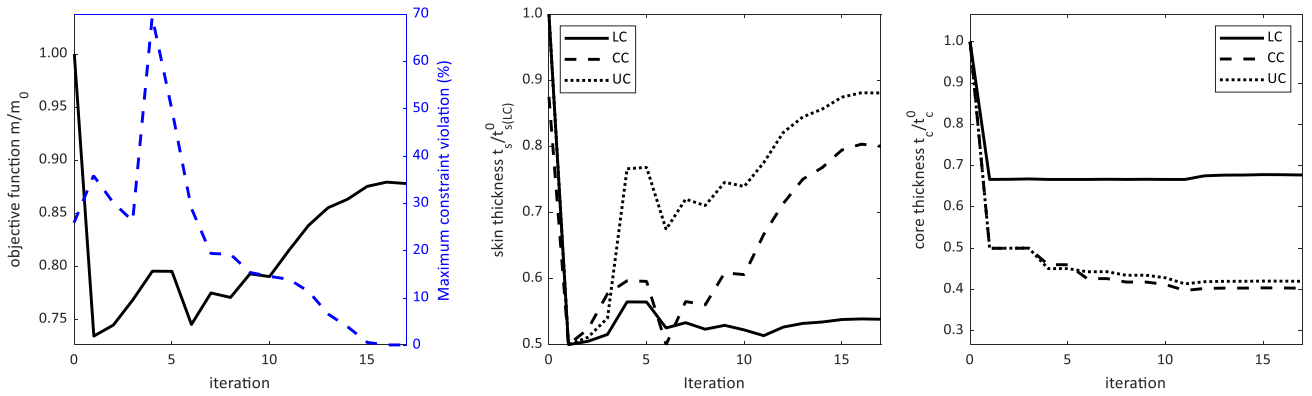

Fig. 7 Step 1 optimization. Constant stiffness substructures. Stiffness constraints only. Convergence plot and evolution of the thickness design variables.

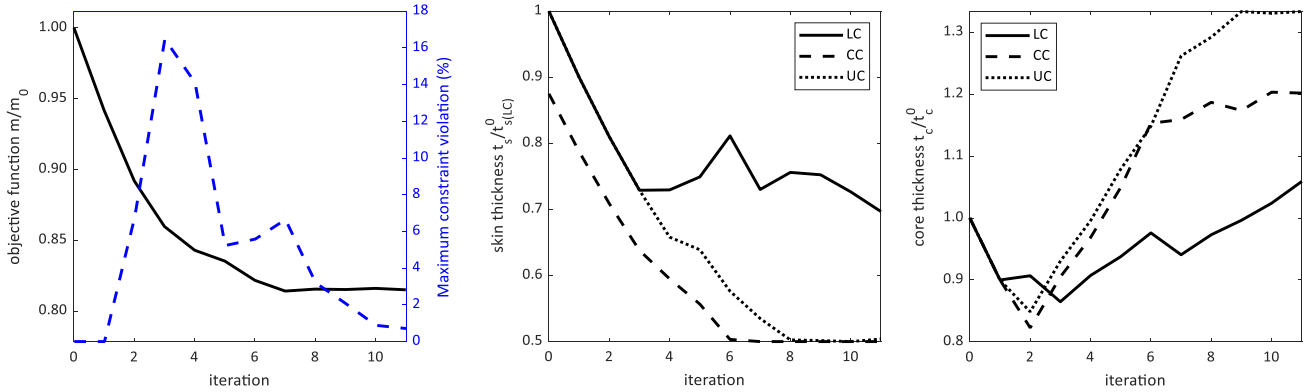

Fig. 8 Step 1 optimization. Constant stiffness substructures. Buckling constraints only. Convergence plot and evolution of the thickness design variables.

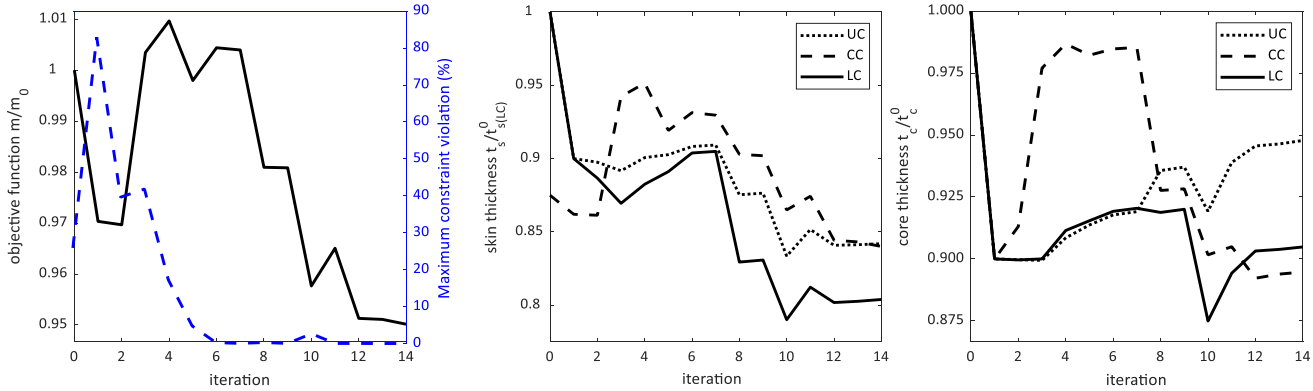

Fig. 9 Step 1 optimization. Constant stiffness substructures. Stiffness and buckling constraints are enforced. Convergence plot and evolution of the thickness design variables.

output corresponds to the results of the FE analysis of the initial design of step 3. The shift in mass between the outputs of steps 1 and 2 is due to the rounding of the skin thickness to the nearest discrete ply number. Between step 2 and 3, the mass variation can be explained by variations of the numbers of plies of the skins, but also by continuous variations of the core thickness. Step 3 output corresponds to the results of the final FE analysis performed using a layer-by-layer description of the sandwich composites, so that all the stiffness matrices **A**, **B**, **D** and **H** are computed using OptiStruct homogenization module and are fully consistent.

In the stiffness-constrained case, one can note that the final result is lighter than the step 1 result, although step 1 optimization is much less constrained than step 3 optimization. This indicates that the result found at step 1 is

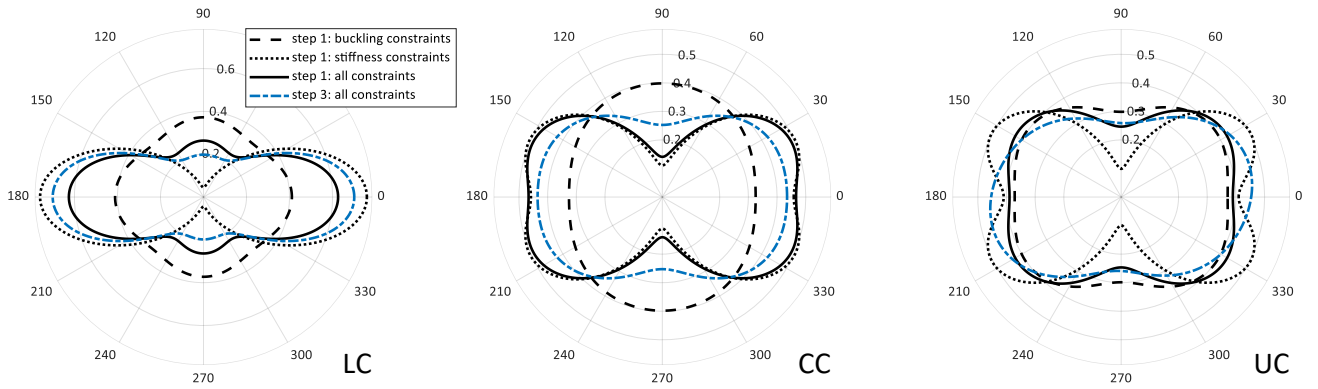

Fig. 10 Step 1 optimization. Constant stiffness substructures. Polar plot of the evolution of the apparent Young's modulus of the skin laminates.

suboptimal. As a matter of fact, the complexity of the optimization problem at hand is twofold. First, the objective function is only related to the thickness design variables. The material anisotropy only influences the value of the constraints. Second, the stiffness constraints are difficult to handle since two stiffness terms have both a lower bound and an upper bound.

In the buckling-constrained case, step 2 optimization returns a design which is far from satisfying the buckling constraints. This difficulty is typical for buckling optimization, since small bending stiffness differences can trigger new buckling modes and have significant influence on the critical buckling loads. Thus, step 3 optimization fails to retrieve a feasible design within the imparted design domain, which is restricted here to ± 1 ply around the skin thicknesses from step 1. A correction of the design based on engineering judgement allows to find a feasible solution by adding one central 0° ply to the skin of the lower cone. This highlights a limitation of the method proposed at step 3. Indeed, if the skin laminate thickness grows higher than the maximum thickness obtained by rounding step 1 results, the choice of the orientation of the additional ply is driven by the laminate design guidelines only. The choice between all the ply orientations that satisfy the guidelines results from the stochastic process of the evolutionary algorithm used at step 2.

When all the constraints are enforced, the optimisation process returns a feasible final design, that is 2.7% heavier than the initial, non-feasible, solution. The optimization problem (20) corresponds to a change of configuration of the SYLDA. Thus, by finding a feasible design, the optimization is successful. When starting from the sandwich composites used for a shorter version of the structure, adding some mass to find a feasible design for the new configuration makes sense. Figure 10 shows the shape of anisotropy of the skin laminates at the end of step 3. The quantity shown in this figure is the apparent Young's modulus of the skin, which is characteristic of the in-plane stiffness matrix $\mathbf{A}$ of the skin. The corresponding laminates are, for the lower cone [15 10 -65 -10 5 -15 -5 65], for the central cylinder [-15 -50 90 -40 50 15 0 40], and for the upper cone [55 5 55 5 -55 -5 -55]. The fit to the target stiffness from step 1 is not perfect. Besides the use of SST for constant-stiffness matching, this discrepancy can be partly explained by the low number of plies, which leads at step 2 to a coarse discretization of the design space with respect to step 1.

It is interesting to note that with constant-stiffness substructures, there is a significant weight penalty for adding one ply to the skin laminates. For instance, with respect to the initial design, adding one ply to the lower cone leads to a 0.8% mass increase. The weight penalty is 1.3% for the upper cone and 5.6% for the central cylinder. This is due to the relative sizes of the substructures and to the fact that the sandwich plates are symmetrical. Hence adding one ply to the skin laminate means adding two plies to the structure itself. Thus, variable thickness skin laminates are necessary to reduce the structural mass.

5.3 Variable-thickness optimization

The composite part of the structure is now divided into 48 zones along its circumference and 21 zones along its length, 2 in the lower cone, 15 in the central cylinder and 4 in the upper cone. The loading and boundary conditions being symmetrical with respect to the (x,z)-plane and the (y,z)-plane, these symmetries are enforced in the definition of the design regions by grouping symmetrical zones. Thus, the lower cone is divided into 24 independent design regions, the central cylinder into 180 design regions and the upper cone into 48 design regions. Each substructure is still assigned to a single value of core thickness, since, practically, a sandwich plate with varying core thickness is unfeasible. Thus, there are 1263 design variables required for step 1, *i.e.* the four membrane lamination parameters

Stiffness-constrained optimization	Mass m/m_0	Maximum constraint violation (%)
Initial design	1.000	25.92
Step 1 output	0.878	0.86
Step 2 output	0.859	4.16
Step 3 output	0.859	0.24 (*)
Buckling-constrained optimization	Mass m/m_0	Maximum constraint violation (%)
Initial design	1.000	25.92
Step 1 output	0.815	0.71 (*)
Step 2 output	0.818	30.8
Step 3 output	0.876	3.2 (failed)
Corrected design	0.886	0.00
All constraints optimization	Mass m/m_0	Maximum constraint violation (%)
Initial design	1.000	25.92
Step 1 output	0.950	0.65 (*)
Step 2 output	0.960	2.32
Step 3 output	1.027	0.00

Table 1 Constant stiffness case. Summary of the optimization results. (*) A 1% tolerance is applied on the maximal constraint violation.

and the skin thickness for each of the 252 design regions, and the core thickness in each substructure.

Step 1 results are illustrated in Figure 11. The figure shows the convergence of the optimization towards a feasible design that is 10.6% lighter than the initial non-feasible solution. The skin laminates of the initial design are balanced, thus V_2^A and V_4^A are null over the entire structure. Their values do not evolve significantly during the optimization, therefore their final distributions are not shown in the figure. This confirms that the optimal laminates tend to be orthotropic, with their orthotropy axes aligned with the longitudianl axis of the SYLDA. This in turn further justifies the choice of working with balanced laminates in step 2. The skin thickness distribution shows two symmetrical thick zones along the length of the central cylinder. Their locations on the circumference of the structure correspond to the location of the maximum axial load due to the booster thrust. The top of the upper cylinder is stiffened by thick skin laminates, due to the presence of the payload.

Figure 12 illustrates the results of the stacking sequence retrieval at step2 and the final thickness and anisotropy distributions after step 3. At step 2, the variable-thickness skin laminate of each substructure is described by a SST. The figure shows the scattering of the skin stiffness terms A_{11}/A_{11}^0 and A_{22}/A_{11}^0 over the 180 regions of the central cone after step 1 optimization, where A_{11}^0 corresponds to the tensor A of the skin laminate of the initial design. Between step 1 and step 2, the skin thickness are rounded. Thus, the feasible design space is discretized with respect to t_s. The convex hull of the feasible design space of the laminate stiffness is shown for integer number of plies only.

All constraints optimization	Mass m/m_0	Maximum constraint violation (%)
Initial design	1.000	25.92
Step 1 output	0.890	0.00
Step 2 output	0.892	14.97
Step 3 output	0.951	0.00

Table 2 Variable skin thickness case. Summary of the optimization results.

This figure highlights a possible limitation of the SST representation. Indeed, in this particular case, no laminate blending constraint is enforced at step 1. Thus, different stiffness properties can be found for regions with the same thickness. However, the use of SSTs at step 2 constrains the design so that a unique laminate is defined for a given number of plies, i.e. a given thickness, even though it might not be justified from a mechanical perspective. Nevertheless, the figure shows how the SST found at step 2 compares with the target from step 1.

Figure 12 shows the final distributions of t_c and t_s and of the lamination parameters V_1^A and V_3^A. Compared to the distributions shown in Figure 11, the skin laminates are thicker. The corresponding weight penalty is partly balanced by the reduction of the core thickness in the lower cone and central cylinder. The V_1^A distributions are very close between the end of step 1 and the final design. The final distribution of V_3^A shows similar, though shallower, variations when compared to step 1.

Table 2 summarizes the optimization results after each optimization step. The final design is about 4.9% lighter than the initial design and 7.4% lighter than the constant stiffness solution. The design is driven by the stiffness and buckling constraints. Although very conservative, the failure criterion was never activated in step 1 or step 3. With a computational time of about 10 s for the FE evaluation of the stiffness criterion and 3 min 40 s for the buckling criterion, the total optimization process lasts about 2 h 30 min. The SST returned by the optimization process are detailed in appendix C. The values of design criteria at the end of each optimization step are given in appendix B. The detail of the design criteria shows that the design is stiffness dominated. Shear crimping, face sheet wrinkling, and intra-cell dimpling are assessed on the final design of the structure, using the closed-form solutions given by [42]. The values of the criteria associated to face sheet wrinkling, and intra-cell dimpling show that these local failure modes clearly are not critical with a margin over 100% everywhere in the design area and for all the considered load cases. The minimal margin with respect to shear crimping is about 35%, which is deemed acceptable at this stage of the sizing process.

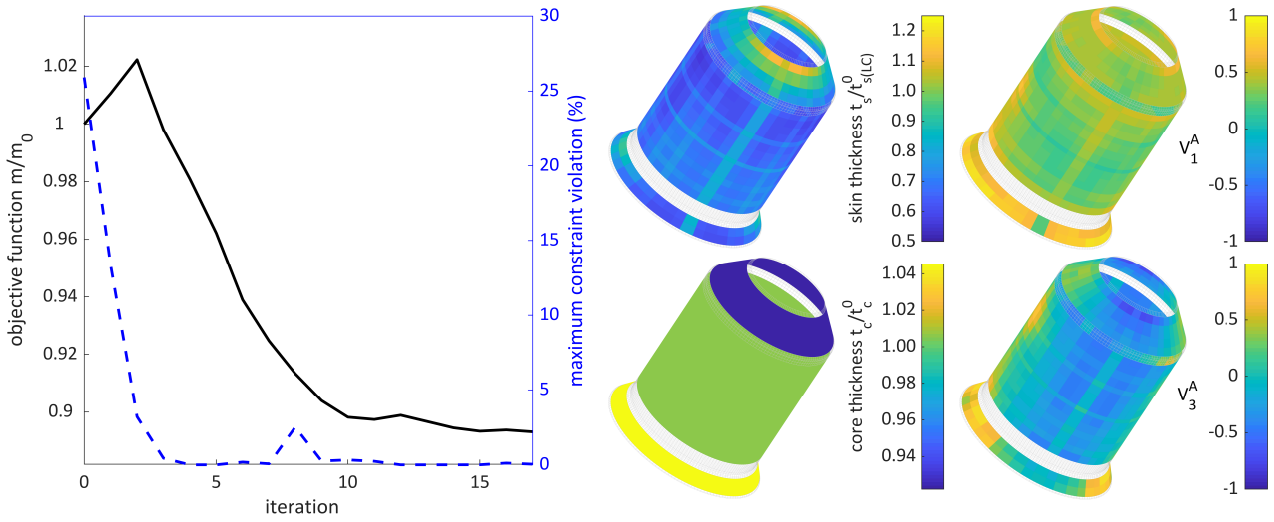

Fig. 11 Step 1 optimization. Variable skin thickness substructures. Convergence plot and design variables output distributions. The output distributions of V_2^A and V_4^A are not shown since they are uniformly close to 0: V_2^A ranges from -0.110 to 0.113 and V_4^A ranges from -0.075 to 0.075.

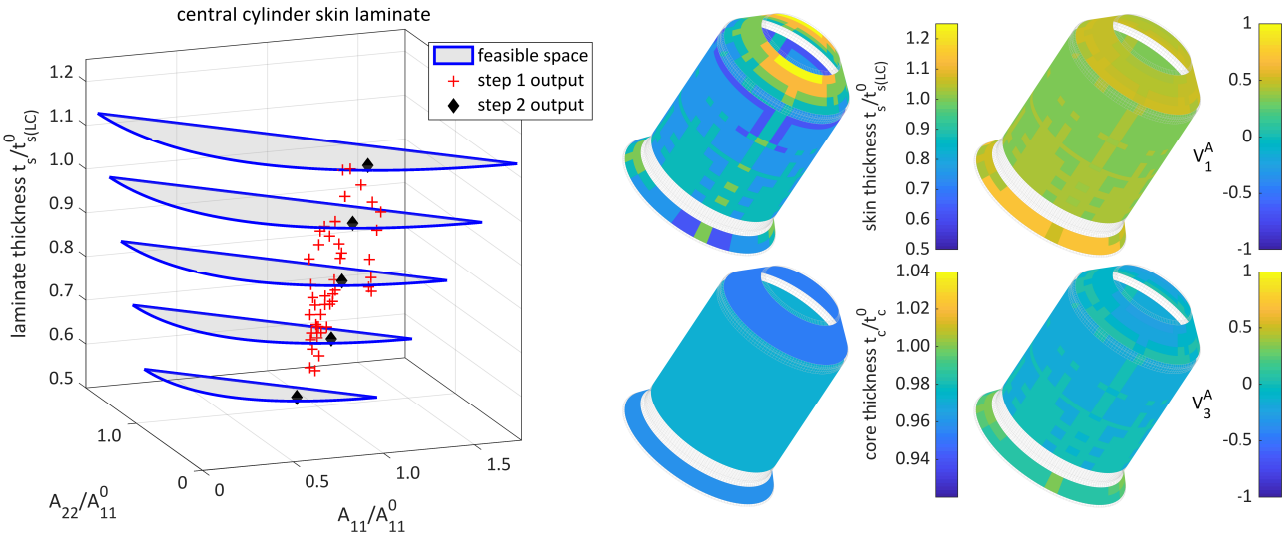

Fig. 12 Step 2 and step 3 optimizations. Variable skin thickness substructures. Comparison between step 1 and step 2 outputs in terms of skin laminate stiffness terms A_{11} and A_{22}. Output distributions of the skin and core thicknesses and V_1^A and V_3^A.

6 Conclusion

This paper presents a three-step optimization strategy for the optimization of sandwich composite structures. The overall process is based on a well-established two-step strategy for laminate optimization to which the present work brings three main novelties.

- First, the lamination parameters scheme is extended to sandwich composites, taking into account the transverse shear stiffness and using a response surface approximation to mimic the homogenization methods implemented in commercial FE software.
- Second, an additional optimization step is proposed to overcome the design feasibility issues related to the use of a stiffness matching method for the retrieval of the stacking sequence of the skins.
- Finally, a numerical procedure is proposed to build an approximate failure envelop formulated on the macroscopic in-plane strains. The method can be applied to any first-ply failure criterion.

The whole strategy has been automated with seamless calls to MSC Nastran or Altair OptiStruct for the structural optimization tasks, the purpose being to provide engineers with a comprehensive design tool.

The efficiency of the proposed approach is shown on a dual-launch system (SYLDA) structure. Starting from the definition of the sandwich composites of reference design, a longer version of the structure is optimized, for mass minimization and feasibility with respect to complex global stiffness requirements, buckling and strength constraints under several load cases. Both constant-stiffness and variable skin thickness optimizations are performed, showing the capabilities of the proposed method on a complex industrial test case.

Replication of Results

A detailed description of the proposed optimization strategy has been provided in this paper, along with the comprehensive implementation details. The authors are thus confident that the overall methodology can be reproduced and, as such, have decided not to publish the code. Due to the particularities of the space industry, some of the data about the application case is omitted. Readers interested in the Python or Matlab scripts are encouraged to contact the corresponding author.

Conflict of Interest Statement

On behalf of all authors, the corresponding author states that there is no conflict of interest.

Appendix

A Variable stiffness optimization case: stacking sequences

At the end of step 2, the SST of the lower cone (LC) is defined by (see Figure 13):
$\mathbf{X_s}$ = [20 0 90 30 -20 80 90 -30 0 -80 20 -20],
$\mathbf{X_i}$ = [0 3 2 0 4 6 8 0 1 7 5 0].
At the end of step 3, the number of plies of the skin laminate ranges from 5 to 8 in the lower cone.

The SST of the central cylinder (CC) is defined by (see Figure 14):
$\mathbf{X_s}$ = [25 40 -5 55 0 -40 0 -55 5 -55 55 -25],
$\mathbf{X_i}$ = [0 4 8 0 2 3 1 0 7 5 6 0].
At the end of step 3, the number of plies of the skin laminate ranges from 5 to 8 in the central cylinder.

Finally, the SST of the upper cone (UC) is defined by (see Figure 15):
$\mathbf{X_s}$ = [-50 -35 20 -40 -5 -35 40 35 -20 35 5 50],
$\mathbf{X_i}$ = [0 7 0 3 1 6 4 8 0 5 2 0].
At the end of step 3, the number of plies of the skin laminate ranges from 6 to 10 in the upper cone.

B Variable stiffness optimization case: design criteria

Table 3 details the results of the variable stiffness optimization case. The values of the design criteria are given for the initial design and the solution at the end of each optimization step. The values indicated for step 2 corresponds to the initial FE analysis performed at the beginning of step 3. Two load cases only induce compression in the SYLDA structure, and buckling is evaluated for these two cases only. $f_{\mathrm{T}}^{(j)}\mathrm{W}$ represents the critical value of the failure constraint (see equation 17) over the design regions of the structure for load case j. The overall design clearly is stiffness dominated.

Design criterion	Initial design	Step 1	Step 2	Step 3
Mass m/m_0	1.000	0.893	0.893	0.951
$\mathrm{K}_{\mathrm{F}_z}^{min}/\mathrm{K}_{\mathrm{F}_z}$	0.873	1.000	1.028	0.903
$\mathrm{K}_{\mathrm{F}_z}/\mathrm{K}_{\mathrm{F}_z}^{max}$	1.005	0.877	0.854	0.972
$\mathrm{K}_{\mathrm{F}_y}^{min}/\mathrm{K}_{\mathrm{F}_y}$	1.350	1.000	1.064	0.980
$\mathrm{K}_{\mathrm{F}_y}/\mathrm{K}_{\mathrm{F}_y}^{max}$	0.648	0.875	0.823	0.892
$\mathrm{K}_{\mathrm{M}_x}^{min}/\mathrm{K}_{\mathrm{M}_x}$	0.788	0.721	0.779	0.692
$\lambda_0^{(1)}/\lambda_1^{(1)}$	0.958	1.002	1.175	0.973
$\lambda_0^{(3)}/\lambda_1^{(3)}$	0.970	0.991	1.175	0.984
$f_{\mathrm{TW}}^{(1)}$	0.034	0.031	0.042	0.031
$f_{\mathrm{TW}}^{(2)}$	0.044	0.041	0.040	0.031
$f_{\mathrm{TW}}^{(3)}$	0.035	0.032	0.043	0.031
$f_{\mathrm{TW}}^{(4)}$	0.030	0.031	0.028	0.023

Table 3 Variable skin thickness case. Detail of the optimization results.

C Variable stiffness optimization case: sandwich failure modes

Shear crimping, face sheet wrinkling, and intra-cell dimpling are checked on the final design of the structure. Proper estimation of these local failure modes would require a detailed finite element analysis, especially in the case of anisotropic face sheet laminates. Following the usual engineering practice, we use here the closed-form solutions derived for uniaxially loaded sandwich panels given by [42].

The local load at which shear crimping occurs is estimated as:

$$\mathrm{N}_{cr} = \mathrm{G}^c t_c, \tag{21}$$

where G_c is the effective transverse shear stiffness of the core material.

The critical value of the local stress for the face wrinkling instability is given by:

$$\sigma_{wr} = \left(\frac{2}{3} \frac{t_s}{t_c} \frac{\mathrm{E}_c \sqrt{\mathrm{E}_x^{(s)} \mathrm{E}_y^{(s)}}}{(1 - \nu_{xy}^{(s)} \nu_{yx}^{(s)})} \right)^{1/2}, \tag{22}$$

with E_c the core effective transverse stiffness, $\mathrm{E}_x^{(s)}$ (resp. $\mathrm{E}_y^{(s)}$) is the macroscopic elastic modulus of the skin laminate in the x-direction (resp. y-direction) and $\nu_{xy}^{(s)}$ and $\nu_{yx}^{(s)}$ are its in-plane Poisson coefficients.

Finally, the critical stress for the face dimpling instability can be written as:

$$\sigma_{di} = \frac{2\sqrt{\mathrm{E}_x^{(s)} \mathrm{E}_y^{(s)}}}{(1 - \nu_{xy}^{(s)} \nu_{yx}^{(s)})} \left(\frac{t_s}{s} \right)^2, \tag{23}$$

with s the cell size of the honeycomb.

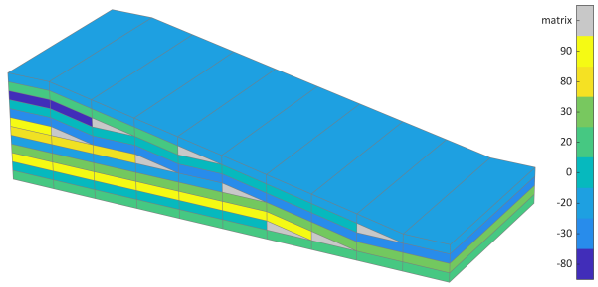

Fig. 13 View of the SST found at step 2 for the lower cone.

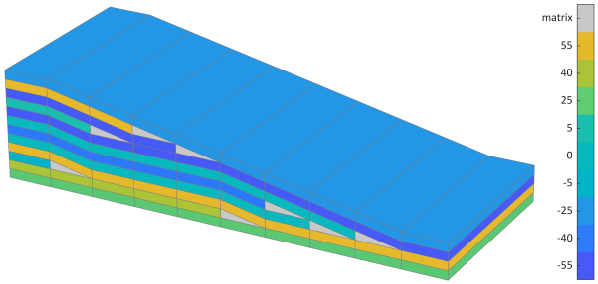

Fig. 14 View of the SST found at step 2 for the central cylinder.

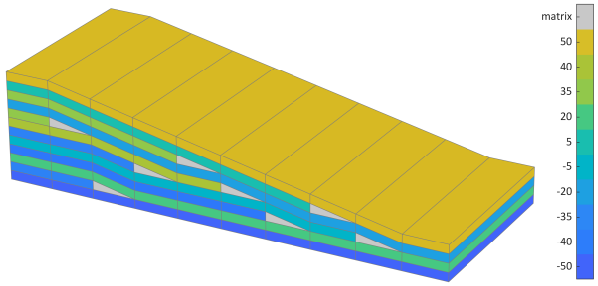

Fig. 15 View of the SST found at step 2 for the upper cone.

References

1. The Basics on Bonded Sandwich Construction. Hexcel technical service bulletin: Hexcel Corp. Hexcel Honeycomb (1986)
2. MSC.Nastran Reference Manual p. 1008 (2014)
3. Abdalla, M.M., Kassapoglou, C., Gürdal, Z.: Formulation of composite laminate robustness constraint in lamination parameters space. In: Proceedings of 50th AIAA/ASME/ASCE/AHS/ASC structures, structural dynamics, and materials conference. Palm Springs, California (2009)
4. Albazzan, M.A., Harik, R., Tatting, B.F., Gürdal, Z.: Efficient design optimization of nonconventional laminated composites using lamination parameters: A state of the art. Composite Structures **209**, 362–374 (2019). DOI 10.1016/j.compstruct.2018.10.095
5. Allen, H.G.: Analysis and Design of Structural Sandwich Panels. Pergamon Press, Kent (1969)
6. Balabanov, V., Weckner, O., Epton, M., Mabson, G., Cregger, S., Blom, A.: Optimal Design of a Composite Sandwich Structure Using Lamination Parameters. In: 53rd AIAA/ASME/ASCE/AHS/ASC Structures, Structural Dynamics and Materials Conference (2012). DOI 10.2514/6.2012-1520
7. Berthelot, J.M.: Composite materials: mechanical behavior and structural analysis. Mechanical engineering series. Springer, New York, NY (1999)
8. Catapano, A., Montemurro, M.: A multi-scale approach for the optimum design of sandwich plates with honeycomb core. Part I: homogenisation of core properties. Composite Structures **118**, 664–676 (2014). DOI 10.1016/j.compstruct.2014.07.057
9. Catapano, A., Montemurro, M.: A multi-scale approach for the optimum design of sandwich plates with honeycomb core. Part II: the optimisation strategy. Composite Structures **118**, 677–690 (2014). DOI 10.1016/j.compstruct.2014.07.058

10. Catapano, A., Montemurro, M.: On the correlation between stiffness and strength properties of anisotropic laminates. Mechanics of Advanced Materials and Structures **26**(8), 651–660 (2019). DOI 10.1080/15376494.2017.1410906
11. Coburn, B.H., Weaver, P.M.: Buckling analysis, design and optimisation of variable-stiffness sandwich panels. International Journal of Solids and Structures **96**, 217–228 (2016). DOI 10.1016/j.ijsolstr.2016.06.007
12. Di Sciuva, M., Gherlone, M., Lomario, D.: Multiconstrained optimization of laminated and sandwich plates using evolutionary algorithms and higher-order plate theories. Composite Structures **59**(1), 149–154 (2003)
13. Diaconu, C.G., Sekine, H.: Layup Optimization for Buckling of Laminated Composite Shells with Restricted Layer Angles. AIAA Journal **42**(10), 2153–2163 (2004). DOI 10.2514/1.931
14. Fan, H.T., Wang, H., Chen, X.H.: Optimization of multi-sandwich-panel composite structures for minimum weight with strength and buckling considerations. Science and Engineering of Composite Materials **25**(2), 229–241 (2018). DOI 10.1515/secm-2015-0171
15. Gantovnik, V.B., Gürdal, Z., Watson, L.T.: A genetic algorithm with memory for optimal design of laminated sandwich composite panels. Composite Structures **58**(4), 513–520 (2002)
16. Ghiasi, H., Fayazbakhsh, K., Pasini, D., Lessard, L.: Optimum stacking sequence design of composite materials Part II: Variable stiffness design. Composite Structures **93**(1), 1–13 (2010). DOI 10.1016/j.compstruct.2010.06.001
17. Ghiasi, H., Pasini, D., Lessard, L.: Optimum stacking sequence design of composite materials Part I: Constant stiffness design. Composite Structures **90**(1), 1–11 (2009). DOI 10.1016/j.compstruct.2009.01.006
18. Haftka, R., Gürdal, Z.: Elements of Structural Optimization. Contributions to Phenomenology. Springer Netherlands (1992)
19. Hammer, V., Bendsøe, M., Lipton, R., Pedersen, P.: Parametrization in laminate design for optimal compliance. International Journal of Solids and Structures **34**(4), 415–434 (1997). DOI 10.1016/S0020-7683(96)00023-6
20. Huang, S., Alspaugh, D.: Minimum Weight Sandwich Beam Design. AIAA Journal **12**(12), 1617–1618 (1974). DOI 10.2514/3.49567
21. Hudson, C.W., Carruthers, J.J., Robinson, A.M.: Multiple objective optimisation of composite sandwich structures for rail vehicle floor panels. Composite Structures **92**(9), 2077–2082 (2010). DOI 10.1016/j.compstruct.2009.10.018
22. IJsselmuiden, S.T., Abdalla, M.M., Gürdal, Z.: Implementation of Strength-Based Failure Criteria in the Lamination Parameter Design Space. AIAA Journal **46**(7), 1826–1834 (2008). DOI 10.2514/1.35565
23. Irisarri, F.X., Abdalla, M.M., Gürdal, Z.: Improved Shepard's Method for the Optimization of Composite Structures. AIAA Journal **49**(12), 2726–2736 (2011). DOI 10.2514/1.J051109
24. Irisarri, F.X., Lasseigne, A., Leroy, F.H., Le Riche, R.: Optimal design of laminated composite structures with ply drops using stacking sequence tables. Composite Structures **107**, 559–569 (2014). DOI 10.1016/j.compstruct.2013.08.030
25. Kawai, M., Saito, S.: Off-axis strength differential effects in unidirectional carbon/epoxy laminates at different strain rates and predictions of associated failure envelopes. Composites Part A: Applied Science and Manufacturing **40**(10), 1632–1649 (2009). DOI 10.1016/j.compositesa.2009.08.007
26. Kodiyalam, S., Nagendra, S., DeStefano, J.: Composite sandwich structure optimization with application to satellite components. AIAA Journal **34**(3), 614–621 (1996). DOI 10.2514/3.13112
27. Koiter, W.T.: The stability of elastic equilibrium. Tech. rep., Stanford Univ Ca Dept of Aeronautics and Astronautics (1970)
28. Leite, P., Thomas, M., Simon, F., Bréchet, Y.: Optimal Design of a Multifunctional Sandwich Panel With Foam Core: Lightweight Design for Flexural Stiffness and Acoustical Transmission Loss. Advanced Engineering Materials **17**(3), 311–318 (2015). DOI 10.1002/adem.201400075
29. Macquart, T., Bordogna, M.T., Lancelot, P., De Breuker, R.: Derivation and application of blending constraints in lamination parameter space for composite optimisation. Composite Structures **135**, 224–235 (2016). DOI 10.1016/j.compstruct.2015.09.016
30. Moakher, M.: On the Averaging of Symmetric Positive-Definite Tensors. Journal of Elasticity **82**(3), 273–296 (2006). DOI 10.1007/s10659-005-9035-z
31. Montemurro, M., Catapano, A., Doroszewski, D.: A multi-scale approach for the simultaneous shape and material optimisation of sandwich panels with cellular core. Composites Part B: Engineering **91**, 458–472 (2016). DOI 10.1016/j.compositesb.2016.01.030
32. Panettieri, E., Montemurro, M., Catapano, A.: Blending constraints for composite laminates in polar parameters space. Composites Part B: Engineering **168**, 448–457 (2019). DOI 10.1016/j.compositesb.2019.03.040
33. Petras, A., Sutcliffe, M.: Failure mode maps for honeycomb sandwich panels. Composite Structures **44**(4), 237–252 (1999). DOI 10.1016/S0263-8223(98)00123-8
34. Picchi Scardaoni, M., Montemurro, M., Panettieri, E., Catapano, A.: New blending constraints and a stack-recovery strategy for the multi-scale design of composite laminates. Structural and Multidisciplinary Optimization (2020). DOI 10.1007/s00158-020-02725-x
35. Reddy, J.N., Reddy, J.N.: Mechanics of laminated composite plates and shells: theory and analysis, 2nd ed edn. CRC Press, Boca Raton (2004)
36. Silva, G.H.C., Meddaikar, Y.: Lamination Parameters for Sandwich and Hybrid Material Composites. AIAA Journal pp. 1–8 (2020). DOI 10.2514/1.J059093
37. Svanberg, K.: The method of moving asymptotes—a new method for structural optimization. International Journal for Numerical Methods in Engineering **24**(2), 359–373 (1987). DOI 10.1002/nme.1620240207
38. Triantafillou, T., Gibson, L.: Failure mode maps for foam core sandwich beams. Materials Science and Engineering **95**, 37–53 (1987). DOI 10.1016/0025-5416(87)90496-4
39. Triantafillou, T.C., Gibson, L.J.: Minimum weight design of foam core sandwich panels for a given strength. Materials Science and Engineering **95**, 55–62 (1987)
40. Tsai, S.W., Hahn, H.T.: Introduction to composite materials. Technomic Pub, Westport, Conn (1980)
41. Velea, M.N., Wennhage, P., Zenkert, D.: Multi-objective optimisation of vehicle bodies made of FRP sandwich structures. Composite Structures **111**, 75–84 (2014). DOI 10.1016/j.compstruct.2013.12.030
42. Vinson, J.R.: Optimum design of composite honeycomb sandwich panels subjected to uniaxial compression. AIAA Journal **24**(10), 1690–1696 (1986). DOI 10.2514/3.9502
43. Wang, T., Li, S., Nutt, S.R.: Optimal design of acoustical sandwich panels with a genetic algorithm. Applied Acoustics **70**(3), 416–425 (2009). DOI 10.1016/j.apacoust.2008.06.003
44. Weckner, O., Balabanov, V.: The Effect of Transverse Shear on the Optimal Design of a Composite Plate. In: 13th AIAA/ISSMO Multidisciplinary Analysis Optimization Conference (2010)
45. Wennhage, P.: Weight Minimization of Sandwich Panels with Acoustic and Mechanical Constraints. Journal of Sandwich Structures & Materials **3**(1), 22–49 (2001). DOI 10.1106/CM4M-7JAY-VBTP-37JE